ADVANCED ELECTRONIC MATERIALS Open Access
www.advelectronicmat.de

Development of Synthetically Accessible Glycolated Polythiophenes for High-Performance Organic Electrochemical Transistors

Bowen Ding, Vianna Le, Hang Yu, Guanchen Wu, Adam V. Marsh, Edgar Gutiérrez-Fernández, Nicolás Ramos, Martina Rimmele, Jaime Martín, Jenny Nelson, Alexandra F. Paterson, and Martin Heeney**

Four glycolated polythiophene-based organic mixed ionic-electronic conductors (OMIECs), PE2gTT, PE2gT, PT2gTT, and PT2gT are prepared by atom-efficient direct arylation polymerization, avoiding the need for toxic organometallic precursors. PE2gT, PT2gTT, and PT2gT are operable in p-type accumulation mode organic electrochemical transistors (OECTs), with PT2gT displaying the best device performance with a μC* product figure-of-merit of 290 F cm^{-1} V^{-1} s^{-1}. A record volumetric capacitance among p-type glycolated polythiophene OMIECs of 313 F cm^{-3} is observed for PE2gT, ascribed to the high proportionality of polar components in its materials design. The good OECT performance of PE2gT with μC* = 84.2 F cm^{-1} V^{-1} s^{-1}, comparable with state-of-the-art poly(3,4-ethylenedioxythiophene):poly(styrenesulfonate) (PEDOT:PSS) devices, coupled with its synthetic accessibility and favorable accumulation mode operation makes PE2gT an ideal glycolated alternative to PEDOT:PSS in bioelectronics. PE2gT with the least negative threshold voltage also displays the best OECT operational cycling stability, linked to better resistance of its oxidized state against parasitic redox side reactions . Shelf life stability of OECTs stored (without bias) is observed to be better for materials with a more negative threshold voltage and higher average molecular weight (PT2gT), that are less susceptible to ambient auto-oxidation and film delamination.

1. Introduction

Contrasting against the traditional solid-state electronics that operate predominantly within the realm of electrons, signal processing in biology employs the concurrent movement of both charges and ions within an aqueous electrolytic environment, giving rise to functional incompatibilities between the two.[1] In order to achieve electronics that interface more effectively with biology, recent research efforts have focussed on the development of bioelectronics, that exploit the mixed conductivity of organic mixed ionic-electronic conductors (OMIECs) to perform signal processing, with potential applications encompassing biosensing, integrated healthcare devices and neuromorphic computing.[2,3] Within bioelectronics, the organic electrochemical transistor (OECT) is the foundational device, that continues to garner significant research attention in

B. Ding, M. Rimmele, M. Heeney
Department of Chemistry and Centre for Processable Electronics
Imperial College London
Molecular Sciences Research Hub (White City Campus)
80 Wood Lane Shepherd's Bush, London W12 0BZ, UK
E-mail: martin.heeney@kaust.edu.sa

V. Le, A. F. Paterson
Department of Chemical and Materials Engineering, and Centre for Applied Energy Research
University of Kentucky
Lexington KY4050, USA
E-mail: alexandra.paterson@uky.edu

The ORCID identification number(s) for the author(s) of this article can be found under https://doi.org/10.1002/aelm.202300580

DOI: 10.1002/aelm.202300580

H. Yu, G. Wu, J. Nelson
Department of Physics and Centre for Processable Electronics
Imperial College London
South Kensington Campus, London SW7 2AZ, UK

A. V. Marsh, M. Heeney
Physical Sciences and Engineering Division (PSE)
King Abdullah University of Science and Technology (KAUST)
Thuwal 23955–6900, Saudi Arabia

E. Gutiérrez-Fernández, N. Ramos, J. Martín
POLYMAT and Polymer Science and Technology Department
Faculty of Chemistry
University of the Basque Country UPV/EHU
Manuel de Lardizabal 3, 20018 Donostia–San Sebastián, Spain

J. Martín
Campus Industrial de Ferrol, CITENI
Universidade da Coruña
Campus Esteiro S/N, Ferrol 15403, Spain

materials development, device optimization, and applications in biosensing.[4–11] Unlike organic field-effect transistors which are gated via a dielectric medium, the modulation of charge-carrying polarons (and bipolarons) throughout the OMIEC active channel of an OECT is achieved through its gate potential induced electrochemical oxidation and reduction, entailing the stoichiometric and volumetric penetration of counterions into the channel material.[12]

OECT operation is often characterized according to Bernard and Malliaras' model, which applies orthogonal ionic and electronic circuits to describe the concurrent movement of both charges and ions within a device.[13] The OECT transconductance, a key figure-of-merit, is derived from Bernard and Malliaras' model to be proportional to the product of active layer volumetric capacitance and charge mobility (μC^*). OECTs can be operated in either accumulation or depletion mode, depending on the electrochemical properties of the active OMIEC material.[14] Accumulation mode OECTs employ OMIECs that have negligible charge carriers in the absence of a gate bias and grow upon increased biasing. Depletion mode devices use materials with sufficient charge carriers to engender intrinsic conductivity, that are depleted through biasing. As OMIECs for depletion mode OECTs are inherently conductive under no gate bias, such devices exhibit higher power consumption, owing to the need for continuously applied gate voltage in order to access and maintain their OFF state.[15] The need for bias to turn devices OFF also contributes to the lower operational stability of depletion mode OECTs in comparison with accumulation mode devices, as biasing to access the OFF state invites the negative impacts of parasitic redox side reactions with water and oxygen.[16–18]

Despite its depletion mode profile, poly(3,4-ethylenedioxythiophene) (PEDOT, most commonly obtained as a water-dispersible two-component blend with anionic poly(styrenesulfonate), i.e., PEDOT:PSS) remains a well-known and popular selection for bioelectronics research in the anodic regime (i.e., p-type).[19] Numerous studies exist that probe the effects of thin film crosslinking, crystallinity, and morphology on device performance and stability.[19–23] To combat electrochemical instability, PEDOT:PSS can be de-doped by reaction with excess alkylamines, to afford neutral PEDOT:PSS that can be operated as an accumulation mode OECT.[18] Biocomposite PEDOT blends with deoxyribonucleic acid (DNA) counteranions have also been developed, with the aim of creating a less acidic and more biocompatible OMIEC.[24] The popularity of PEDOT can (at least in part) be attributed to its ease of synthesis and availability. Commercial PEDOT:PSS is made by the oxidative polymerization of 3,4-ethylenedioxythiophene (EDOT) in the presence of PSS, whilst electropolymerization of EDOT can also be performed to create OECT channels of tunable characteristics.[25,26]

Building on the success of PEDOT, there has been recent growth in the materials design of single-component polythiophene-based p-type OMIECs for OECTs.[27–31] Single-component OMIECs afford specific advantages including stronger ionic-electronic coupling and higher volumetric capacitances when compared to their multi-component brethren.[32] In order to engender ionic conductivity into a single-component organic semiconductor, polar sidechains are incorporated. Earlier studies mostly focussed on the attachment of ionic sidechains, to create conjugated polyelectrolytes (CPEs).[33–36] However, much like PEDOT:PSS itself, these CPEs often exhibit aqueous solubility, necessitating the application of performance-diminishing crosslinkers in their OECT channels.[6,33,37] As such, research attention shifted towards developing polythiophenes with oligomeric ethylene glycol sidechains, that enable ion conduction without conferring aqueous solubility.[38] Seeded from the seminal studies by Giovannitti et al. and Nielsen et al. that describe **P(g2T-TT)** and **P(g2T-T)** respectively,[39,40] there is now an expanding library of high-performance p-type glycolated polythiophene based OMIECs. Materials design studies have explored modifications to both sidechain and backbone configuration, for example in altering sidechain distribution,[41] adopting propylene and butylene glycol substitutes,[42] as well as incorporating the cyclopentadithiophene unit,[43] to attain OECT μC^* product performances of 322, 342 and 370 F cm^{-1} V^{-1} s^{-1} respectively. However, most of these glycolated polythiophenes require multistep syntheses employing Stille polymerization, which is undesirable from both an upscaling and toxicity point of view.

Drawing inspiration from the high OECT performances attainable with glycolated polythiophenes, as well as the prevalence of PEDOT in bioelectronics, we designed a set of glycolated polythiophene-based OMIECs with systematic change in their materials design by the co-polymerization of either thiophene (**T**) or the more electron rich EDOT (**E**), with doubly glycolated co-monomers based on thiophene (**2gT**) and thieno[3,2-b]thiophene (**2gTT**). The incorporation of two triethylene glycol sidechains in **2gT** and **2gTT** aims to facilitate the volumetric penetration of counterions into films of resulting co-polymers, without conferring undesirable aqueous solubility and causing undue compromise to electronic charge conduction pathways. Designed variability of the proportion of polar glycol sidechains (and ethylenedioxy bridges) in each polymeric repeat unit was expected to lead to diverse volumetric capacitances and swelling characteristics that can also impact OECT performance.

The resulting **PE2gTT**, **PE2gT**, **PT2gTT**, and **PT2gT** materials were synthesized according to a streamlined scheme employing atom-efficient direct arylation polymerizations that also circumvents the need for toxic organometallic precursors. Electrochemistry revealed onsets of oxidation at −0.5, −0.7, −0.2, and 0.3 V versus Ag/AgCl for **PE2gTT**, **PE2gT**, **PT2gTT**, and **PT2gT** respectively. **PT2gT** displayed the overall champion accumulation mode OECT performance with a μC^* product figure-of-merit of 290 F cm^{-1} V^{-1} s^{-1}, ascribed to its high degree of polymerization that enable its superior charge mobility at 1.00 cm^2 V^{-1} s^{-1}. **PE2gT** exhibited a record volumetric capacitance among p-type glycolated polythiophene OMIECs of 313 F cm^{-3}, attributed to the high proportion of polar glycol and ethylenedioxy components in its materials design. The good OECT performance of **PE2gT**, with a μC^* figure-of-merit of 84.2 F cm^{-1} V^{-1} s^{-1} that is comparable with state-of-the-art PEDOT:PSS devices, coupled with its synthetic accessibility and favorable intrinsic accumulation mode operation makes **PE2gT** a suitable glycolated alternative to PEDOT:PSS in bioelectronics. **PE2gT** with the least negative threshold voltage also displayed the best OECT cycling performance, owing to better resistance of its oxidized state against redox side reactions with products of the oxygen reduction reaction (ORR), whilst shelf life stability was found to be best for **PT2gT** with the

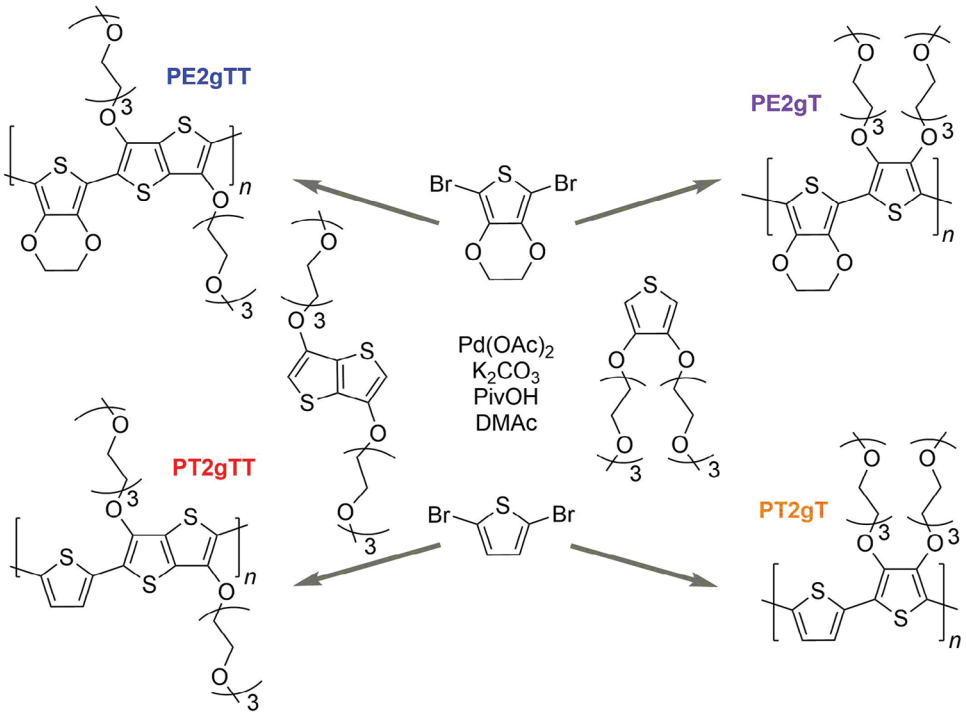

Scheme 1. Direct arylation polymerization of **PE2gTT**, **PE2gT**, **PT2gTT** and **PT2gT**.

most negative threshold voltage and highest average molecular weight, due to greater material resistance against ambient auto-oxidation and film delamination.

2. Results and Discussion

2.1. Synthesis and Macromolecular Properties

The direct arylation polymerizations of 2,5-dibromo-3,4-ethylenedioxythiophene (**E**) and 2,5-dibromothiophene (**T**) with unsubstituted 3,6-bis(triethyleneglycolmonomethylether)-thieno[3,2-*b*]thiophene (**2gTT**) and 3,4-bis(triethyleneglycolmonomethylether)thiophene (**2gT**), to give **PE2gTT**, **PE2gT**, **PT2gTT**, and **PT2gT** (**Scheme 1**), were conducted in ligand-free conditions similar to that reported previously by Sommer and coworkers,[44–46] circumventing the need for synthetic conversion of monomers to toxic organometallic polymerization precursors. Crude polymers were purified by sequential washings with hot solvent to remove impurities and low-weight material. Following reprecipitation, **PE2gT**, and **PT2gT** were obtained in excellent yields of 80% and 76% respectively, whereas yields of thienothiophene incorporating **PE2gTT** and **PT2gTT** were significantly lower at 30% and 28%. Attempts at improving the yield of **PE2gTT** and **PT2gTT** by switching from dimethylacetamide to aromatic solvents (i.e., chlorobenzene and toluene),[47,48] increasing reaction temperature as well as the incorporation of the tri(*o*-anisole) phosphine ligand[49] proved unsuccessful, resulting in poor solubility of polymers, crosslinked products, and extremely low weight oligomeric species respectively.

The structural identities of **PE2gTT**, **PE2gT**, **PT2gTT**, and **PT2gT** were confirmed through a combination of hot ^{1}H NMR at 65 °C as well as the fragmental analysis of their matrix-assisted laser desorption/ionization (MALDI) mass spectrometry traces (Figures S1–S8, Supporting Information). Interpretation of **PE2gTT**, **PE2gT**, **PT2gTT**, and **PT2gT** IR spectra were complicated by the overpowering presence of glycol sidechain signals (Figure S9, Supporting Information). However, for **PT2gTT** and **PT2gT** a signal at 3040 cm^{-1} was seen and assigned to C-H stretching on the 3- and 4- positions of the unsubstituted thiophene present in the repeating unit of both materials. No signal near 3040 cm^{-1} was seen for **PE2gTT** and **PE2gT** featuring 3,4-disubstituted EDOT in place of unsubstituted thiophene. Gel permeation chromatography (GPC) was applied to probe the macromolecular sizes of all four polymers (**Table 1**; Figures S10–S13, Supporting Information), revealing a $M_n/Đ$ of 11 KDa/2.0 and 50 KDa/3.8 for **PT2gTT** and **PT2gT** respectively, against polystyrene standards. Analysis of **PE2gTT** and **PE2gT** molecular weights by GPC was complicated by their tendency to aggregate in solution (owing to backbone auto-oxidation in air), with examination of UV detector responses suggesting an unrealistically broad $M_n/Đ$ of 3.1 KDa/31 and 4.1 KDa/34 for

Table 1. Macromolecular properties of **PE2gTT**, **PE2gT**, **PT2gTT**, and **PT2gT**.

Material	M_n [KDa]	Đ	Determination Method
PE2gTT	3.0	–	NMR
PE2gT	3.6	–	NMR
PT2gTT	11	2.0	GPC (RI)
PT2gT	50	3.8	GPC (RI)

Table 2. Electronic and optical properties of **PE2gTT**, **PE2gT**, **PT2gTT,** and **PT2gT**.

Material	$HOMO_{DFT}$ [eV]	$LUMO_{DFT}$ [eV]	$E_{g,DFT}$ [eV]	Onset of Oxidation [V vs Ag/AgCl]	HOMO [eV][a)]	Onset of Absorption [nm]	$E_{g,opt}$ [eV]	LUMO [eV][b)]
PE2gTT	−4.22	−1.79	2.43	−0.5	−4.1	640	1.9	−2.2
PE2gT	−4.09	−1.54	2.55	−0.7	−3.9	700	1.8	−2.1
PT2gTT	−4.58	−2.07	2.51	−0.2	−4.4	620	2.0	−2.4
PT2gT	−4.51	−1.87	2.64	0.3	−4.9[c)]	610	2.0	−2.9

[a)] Calculated from the onset of electrochemical oxidation, by assuming the Ag/AgCl process occurs at −4.6 eV; [b)] Estimated by adding optical bandgap to corresponding HOMO energy level; [c)] Discrepancy with DFT computed HOMO caused by constriction of counterion diffusion.

PE2gTT and **PE2gT** respectively. Integration analysis of their hot ^{1}H NMRs indicated average molecular weights of 3.0 and 3.6 KDa for **PE2gTT** and **PE2gT** respectively, confirming their low degree of polymerization, equivalent to an average chain length of five to seven repeating units. The lower degree of **PE2gTT** and **PE2gT** polymerization may be explained by their tendency to auto-oxidize upon heating (see below paragraph discussing UV/Vis traces), which potentially compromises the Pd(0) catalytic cycle.[50] No thermal processes were recorded between 40 – 300°C in the differential scanning calorimetry traces of **PE2gTT**, **PE2gT**, **PT2gTT,** and **PT2gT** (Figures S14–S17, Supporting Information).

2.2. Optical and Electronic Properties

Density functional theory (DFT) computations of **PE2gTT**, **PE2gT**, **PT2gTT,** and **PT2gT** trimeric models were conducted at the B3LYP/6-31G(d,p) level of theory to probe the energetics and physical conformation of their materials design. The DFT energetics of all four polymers are summarized in **Table 2**. It is evident polymers with a higher ratio of aryl ether substitutions per thiophene unit are calculated to have shallower HOMO levels (**PT2gTT** < **PT2gT** < **PE2gTT** < **PE2gT**), owing to the mesomeric electron-donating effect of aryl ether linkages into the backbone. All four polymers are predicted to feature highly planar backbones that are required for good orbital delocalization and charge transport, achieved through the incorporation of favorable S...O non-covalent interactions (Figures S18–S33, Supporting Infromation).[51]

The solution state UV/Vis of **PE2gTT**, **PE2gT**, **PT2gTT,** and **PT2gT** in chloroform (Figures S34–S38, Supporting Infromation) all showed evidence of polymer aggregation, with their S0-S1 transitions at λ_{max} = 552, 583, 529, and 528 nm respectively exhibiting red-shifted shoulders, that dissipate upon warming for **PT2gTT** and **PT2gT**. Low energy polaron bands at 780 and 760 nm were identified in the UV/Vis traces of **PE2gTT** and **PE2gT** respectively, that intensified upon heating in ambient atmosphere. This suggests **PE2gTT** and **PE2gT** can both be oxidized (i.e., doped) in the as-synthesized "resting" state. Polaron bands were not observed for **PT2gTT** and **PT2gT**, including at elevated temperatures. The optical bandgaps of **PE2gTT**, **PE2gT**, **PT2gTT,** and **PT2gT** were estimated from their onsets of S0-S1 absorption in the solution state, to be 1.9, 1.8, 2.0, and 2.0 eV respectively. UV/Vis of **PE2gTT**, **PE2gT**, **PT2gTT,** and **PT2gT** thin films showed broadened transitions when compared against the solution state, which is explained by packing effects in the solid state (Figure S39, Supporting Information).

The aqueous thin film electrochemistry of all four polymers was recorded in 0.1 M KCl/H_2O (**Figure 1**). Cyclic voltammetry (CV) and square wave voltammetry (SQW) experiments revealed **PE2gTT**, **PE2gT**, **PT2gTT,** and **PT2gT** onsets of oxidation at −0.5, −0.7, −0.2 and 0.3 V versus Ag/AgCl respectively. The HOMOs of **PE2gTT**, **PE2gT**, **PT2gTT,** and **PT2gT** were calculated to lie at −4.1, −3.9, −4.4, and −4.9 eV respectively, by assuming the Ag/AgCl process occurs at −4.6 eV, which for **PE2gTT**, **PE2gT,** and **PT2gTT** are in good agreement with DFT calculations. The slight difference between onset of **PT2gT** electrochemical oxidation and its HOMO level from DFT may be explained by the swelling behavior of its films (see Discussion on Device Performance and Thin Film Microstructure and Swelling sections); electrochemical quartz crystal microbalance (EQCM, Figure 5a) measurements on **PT2gT** films revealed minimal electrolyte swelling at potentials more cathodic than ≈0.5 V versus Ag/AgCl, impacting counterion diffusion within **PT2gT** films, reasoning the observed discrepancy between its oxidation onset and calculated HOMO.[52] Despite this, the volumetric penetration of counterions into thin films of **PE2gTT**, **PE2gT**, **PT2gTT,** and **PT2gT** upon bulk electrochemical oxidation was confirmed through scan rate dependence CV data, that revealed the diffusion-limited nature of their electrochemical oxidation in accordance with the Randles-Sevcik equation.[53] CV cycling for 12 scans were applied to confirm the excellent electrochemical stability and reversibility of all four polymers (Figures S40–S43, Supporting Information). To complement aqueous electrolyte results, the electrochemistry of all four polymers was also recorded in 0.1 M $[n\text{-}Bu_4N]PF_6$/MeCN, revealing similar oxidatively active behaviors (Figures S44–S57, Supporting Information).

In order to identify the nature of their electrochemically oxidized states, thin films of all four polymers were also probed by UV/Vis spectroelectrochemistry (SEC) in 0.1 M KCl/H_2O. For **PT2gTT** thin films (**Figure 2**), upon application of a potential of −0.2 V versus Ag/AgCl, which was incremented anodically to 0.5 V, a gradual quenching of the polymer ground state transitions was observed concurrent with the appearance of a polaron band at 850 nm. As the applied potential was further incremented above 0.5 V, to 0.8 V, a reduction in polaron and (remaining) ground state transition intensities were observed, which is consistent with bipolaron formation.[54] Reversing the applied potential incrementally back to −0.2 V resulted in the initial re-intensification of polaron state transitions, followed by the restoration of ground state spectra, indicating full electrochemical reversibility of polaronic and bipolaronic states. Thus, the UV/Vis SEC of **PT2gTT** indicates the

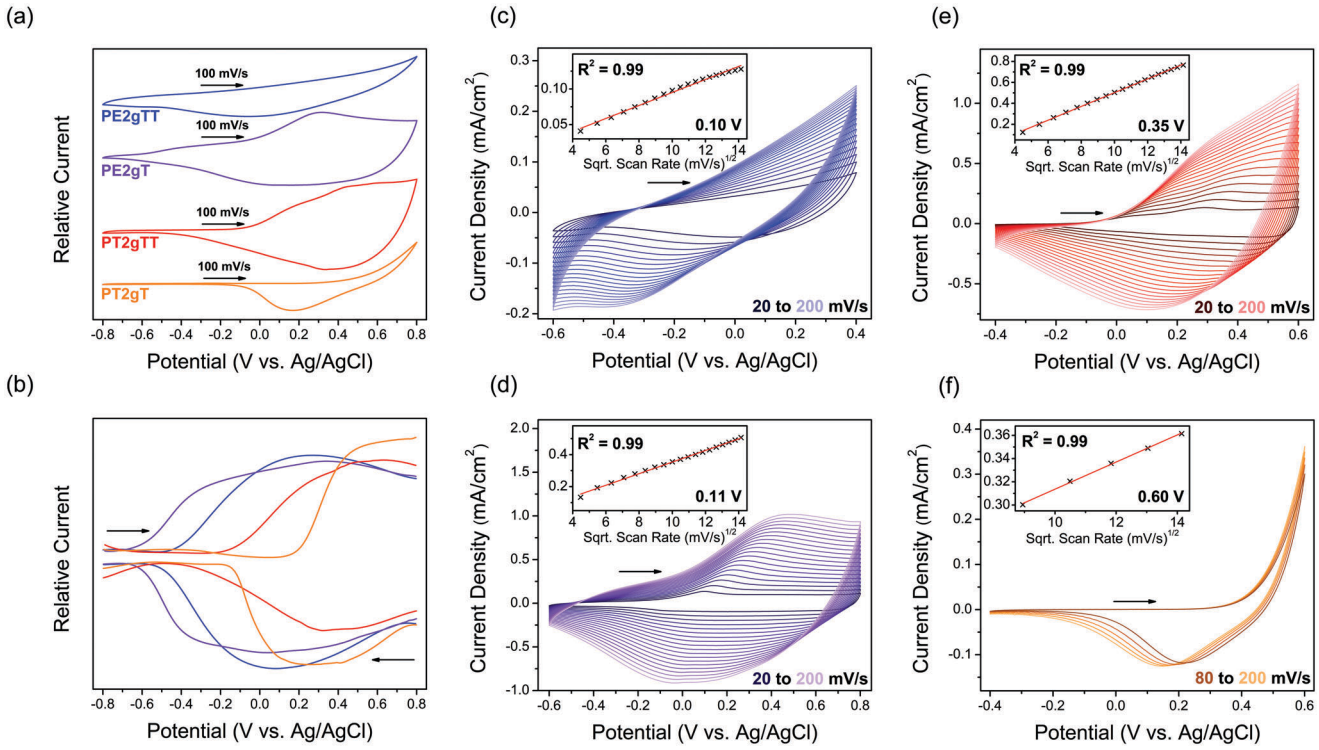

Figure 1. Thin film electrochemistry in 0.1 $_{M}$ KCl/H_2O of **PE2gTT** (blue), **PE2gT** (violet), **PT2gTT** (red) and **PT2gT** (orange) showing a) CV, b) SQW and c–f) scan rate dependence CV, with insets showing plots of currents at (c) 0.10 (d) 0.11 (e) 0.35, and (f) 0.60 V versus Ag/AgCl against the square root of scan rates (linear regression in red). Arrows indicate scan direction.

reversible accession of polaron and bipolaron charge carriers on its backbone at anodic potentials above −0.2 and 0.5 V respectively. Similarly, reversible generation of both polarons and bipolarons on **PE2gTT**, **PE2gT**, and **PT2gT** backbones were also observed in their UV/Vis SEC (Figures S58–S69, Supporting Information), at onset potentials which are summarized in **Table 3**.

2.3. OECT Performance

Fabrication of OECTs with all four polymers **PE2gTT**, **PE2gT**, **PT2gTT**, and **PT2gT** was attempted, however ambient operability in 0.1 M KCl/H_2O was observed for **PE2gT**, **PT2gTT**, and **PT2gT** only. Channel delamination of **PE2gTT** OECTs occurred upon contact with aqueous electrolyte, irrespective of post-treatment (annealing) procedures, preventing its stable device operation, which may relate to its low molecular weight. For **PE2gT**, **PT2gTT**, and **PT2gT** p-type accumulation mode OECTs, their performance was interpreted using the transconductance expression (Equation 1, **Table 4**, **Figure 3**; Figures S70–S74, Supporting Information; V_G = gate voltage, I_D = drain current).[12] V_G is interpreted relative to the Ag/AgCl reference potential, where negative V_G corresponds to oxidative biasing of channel materials.

$$g_m = \frac{\partial I_D}{\partial V_G} = \mu C^* \frac{Wd}{L}\left(V_{Th} - V_G\right) \quad (1)$$

Overall, **PT2gT** OECTs exhibited the best performance, achieving an excellent μC* figure-of-merit benchmark of 290 F cm^{-1} V^{-1} s^{-1}, which can be attributed to its large volumetric capacitance of 290 F cm^{-3}, that is balanced against a good charge mobility calculated at 1.00 cm^2 V^{-1} s^{-1}. An even higher volumetric capacitance of 313 F cm^{-3} was attained in **PE2gT** OECTs, that is a record among p-type glycolated OMIECs (Table S1, Supporting Information), however, its overall modest μC* figure-of-merit of 84.2 F cm^{-1} V^{-1} s^{-1} corresponds with a lower calculated charge mobility at 0.270 cm^2 V^{-1} s^{-1}, offsetting any performance advantages afforded by its exceptional volumetric capacitance. The observed V_{Th} of **PE2gT** accumulation mode OECTs (−0.106 V) is at a noticeably more oxidative potential compared to its electrochemical onset of oxidation measured under inert atmosphere, indicating that generation of stable electronic charge carriers (holes) in **PE2gT** thin films to a sufficient concentration to facilitate electronic conductivity can only be achieved at anodic potentials above 0.1 V versus Ag/AgCl. **PT2gTT** exhibited the poorest (accumulation mode) OECT performance among the trio of polymers tested, with a μC* figure-of-merit of 61.2 F cm^{-1} V^{-1} s^{-1}, owing to a relatively lowercharge mobility calculated at 0.277 cm^2 V^{-1} s^{-1} and volumetric capacitance of 221 F cm^{-3}. All OECTs displayed commendable ON/OFF ratios at factors of 10^4.

The OECT performance of **PT2gT** is comparable with the current state-of-the-art glycolated polythiophene based p-type OECT materials (Table S1, Supporting Information), and on par with the most prevalent design, **P(g2T-TT)**.[27,39–43,55–57] **PE2gT**, **PT2gTT**, and **PT2gT** all achieve volumetric capaci-

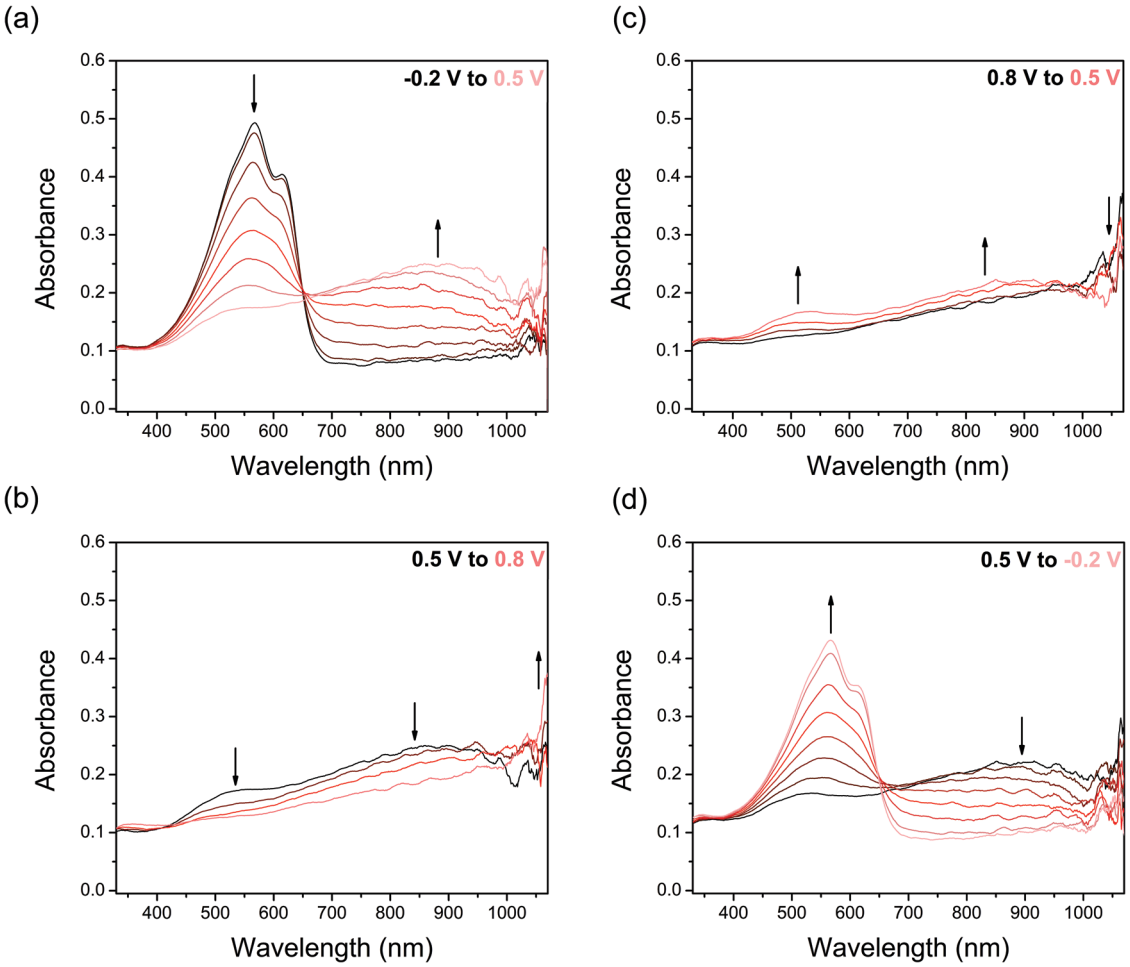

Figure 2. UV/Vis SEC of **PT2gTT** thin films in 0.1 $_M$ KCl/H_2O showing spectral changes upon applying an increasingly anodic potential from a) −0.2 to 0.5 V versus Ag/AgCl and from b) 0.5 to 0.8 V, as well as upon returning the applied potential from c) 0.8 to 0.5 V and from d) 0.5 to −0.2 V. Arrows indicate spectral progression. Incrementation of potentials was conducted at 0.1 V intervals.

tances that are among the highest reported for p-type glycolated OMIECs (Table S1, Supporting Information), with further augmentation possible through electrolyte and morphology optimization,[7,55,58–60] which sets the precedent for their potential application in energy storage, in addition to their use in bioelectronics.[54]

The shelf lives of **PE2gT**, **PT2gTT,** and **PT2gT** OECTs were investigated by comparing peak source-drain currents attained with freshly fabricated versus two-day-aged devices. The ratio of peak currents attained with new versus aged devices were calculated to represent active material shelf life stability and are plot against the corresponding threshold voltages of new devices in Figure 3e, to illustrate the correlation between glycolated polythiophenes of a more negative OECT threshold voltage displaying improved shelf lives, owing to better material resistance against ambient auto-oxidation.[16,61] OECT shelf life stabilities also reflect the average molecular weights of each active material; **PT2gT** with the highest M_n had the best shelf life stability, whereas **PE2gT** with poorer shelf life stability had the lowest M_n. Shelf life stability of **PE2gT** OECTs was observed to be compromised by channel delamination (Figure S75, Supporting Information), which contextualized with the OECT inoperability of **PE2gTT**, leads to the proposition that OECT shelf life stability is optimal for high molecular weight OMIECs with the best film-forming properties and strongest resistance against ambient auto-oxidation.[62] Additionally, operational device stabilities of **PE2gT**, **PT2gTT,** and **PT2gT** were investigated by OECT cycling measurements, by recording the linear and saturation transfer characteristics every 6 seconds for over 300 cycles (Figure S76, Supporting

Table 3. Onset potentials for accessing polaron and bipolarons states on **PE2gTT**, **PE2gT**, **PT2gTT,** and **PT2gT**, as revealed by their thin-film UV/Vis SEC in 0.1 $_M$ KCl/H_2O.

Material	Onset of Polaron [V vs Ag/AgCl]	Onset of Bipolaron [V vs Ag/AgCl]
PE2gTT	−0.5	0.3
PE2gT	−0.7	0.2
PT2gTT	−0.2	0.5
PT2gT	0.3	0.7

Table 4. OECT performance metrics. Width/length (W/L) of channel was 250/50 µm for all devices.

Material	D [nm][a)]	V_{Th} [V][b)]	I_{ON}/I_{OFF}[c)]	g_m [S cm^{-1}][d)]	µC* [F cm^{-1} V^{-1} s^{-1}][e)]	C* [F cm^{-3}, EIS][f)]	μ [cm^2 V^{-1} s^{-1}][g)]
PE2gT	61.2 ± 4.8	−0.106 ± 0.012	10^4	183.8 ± 56.6	84.2 ± 27	313	0.270 ± 0.086
PT2gTT	116 ± 21	−0.302 ± 0.014	10^4	105.5±26.5	61.2 ± 12	221	0.277 ± 0.056
PT2gT	127 ± 3	−0.540 ± 0.008	10^4	253.1±18.4	290 ± 80	290	1.00±0.278

[a)] Channel thickness; [b)] Threshold voltage; [c)] ON/OFF ratio; [d)] Transconductance normalized against channel thickness; [e)] µC* determined by the product of C* obtained from EIS and μ calculated from peak transconductance; [f)] Volumetric capacitance, measured by EIS (electrochemical impedance spectroscopy, using a conventional 3-electrode system); [g)] Charge mobility calculated by dividing volumetric capacitance (C*) from the figure-of-merit (µC*) determined using peak transconductance.

Information), with switching of gate voltage to −0.7 V for **PE2gT** as well as −0.8 V for **PT2gTT** and **PT2gTT**, to replicate aggressive cycling conditions that reach beyond the peak transconductance states of each material, thereby rigorously probing operational cycling behaviors.[16,63] Of the three polymers, **PE2gT** OECTs demonstrated the best operational cycling stability, retaining 34% of its initial source-drain current on its 333rd cycle (2000 s). On the other hand, **PT2gTT** and **PT2gT** retained 0.12% and 0.05% of their respective initial source-drain current on the 333rd cycle. The OECT operational stabilities of **PE2gT**, **PT2gTT**, and **PT2gT** thus follow the reverse correlation to that for shelf life stability, where materials of a higher threshold voltage/more cathodic oxidation onset show better operational cycling stabilities. This is explained by better energetic resistance of the oxidized state of glycolated polythiophenes with more cathodic oxidation onsets, against parasitic redox side reactions with products of the ORR, notably hydroxide, occuring at the OECT drain in the OFF state, as characterised previously.[63]

2.4. Thin Film Microstructure and Swelling

To investigatethe effects of their thin film microstructure on OECT performance, the grazing-incidence wide-angle X-ray scattering (GIWAXS) profiles of all four polymers were collected (**Figure 4**). **PT2gTT** thin films exhibited bimodal crystal orientation, with "lamellar" peaks (100) (at q = 3.3 nm^{-1}, *d-spacing* = 1.9 nm) and π–π stacking peaks (at q = 17.3 nm^{-1}, *d-spacing* = 0.36 nm) showing up along both q_r and q_z directions. **PE2gT** thin films displayed marginal preference to interact face-on with the substrate, as characterized by orientation of the π–π reflection

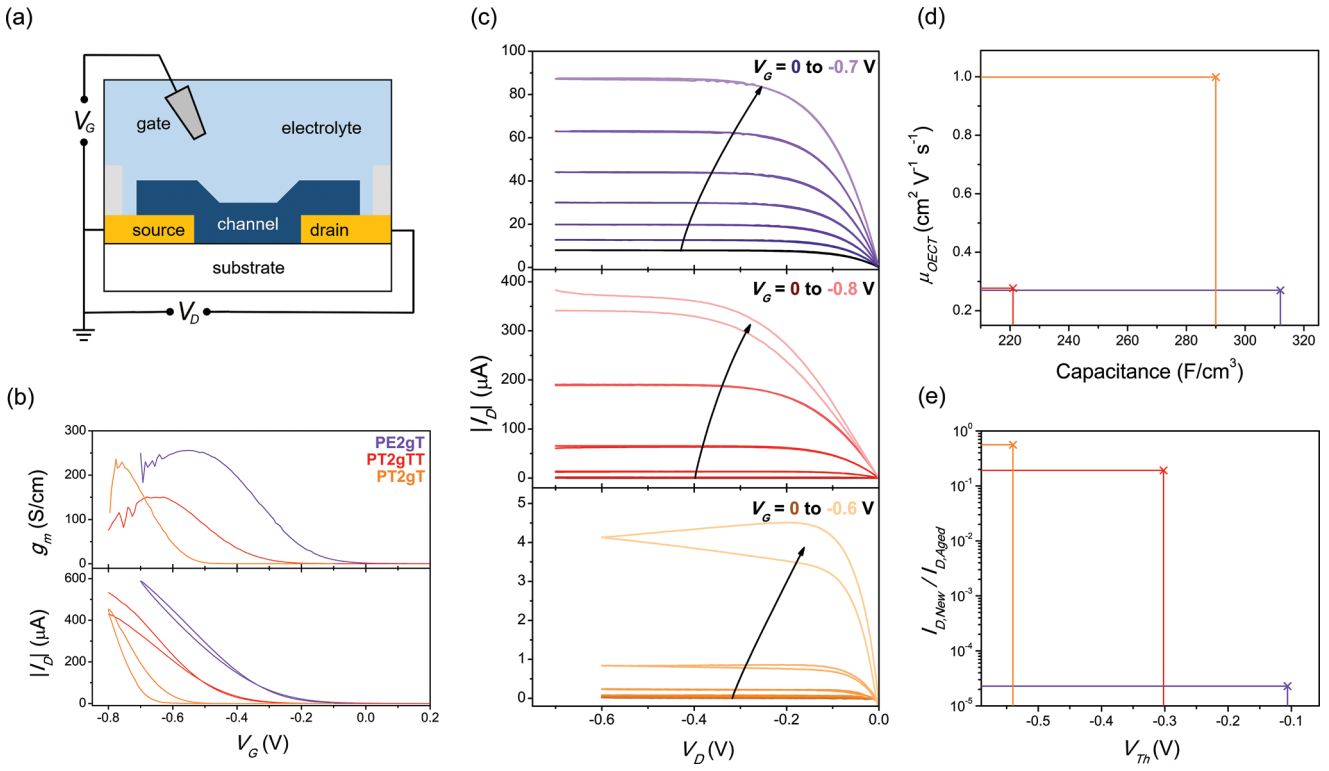

Figure 3. OECT performance of **PE2gT** (violet), **PT2gTT** (red) and **PT2gT** (orange) showing a) device architecture; b) channel thickness normalized transconductance (top, transconductance used to calculate µC*) and transfer curves at V_D = −0.7 V (bottom); c) OECT output curves at stepped V_G in 0.1 V intervals within indicated ranges (arrows indicate data at more negative/channel oxidative V_G); d) plot of volumetric capacitances against OECT mobilities; and e) OECT shelf life stabilities of each material (quantified by the loss of peak source-drain currents between new versus aged devices), plot against corresponding threshold voltages of new devices.

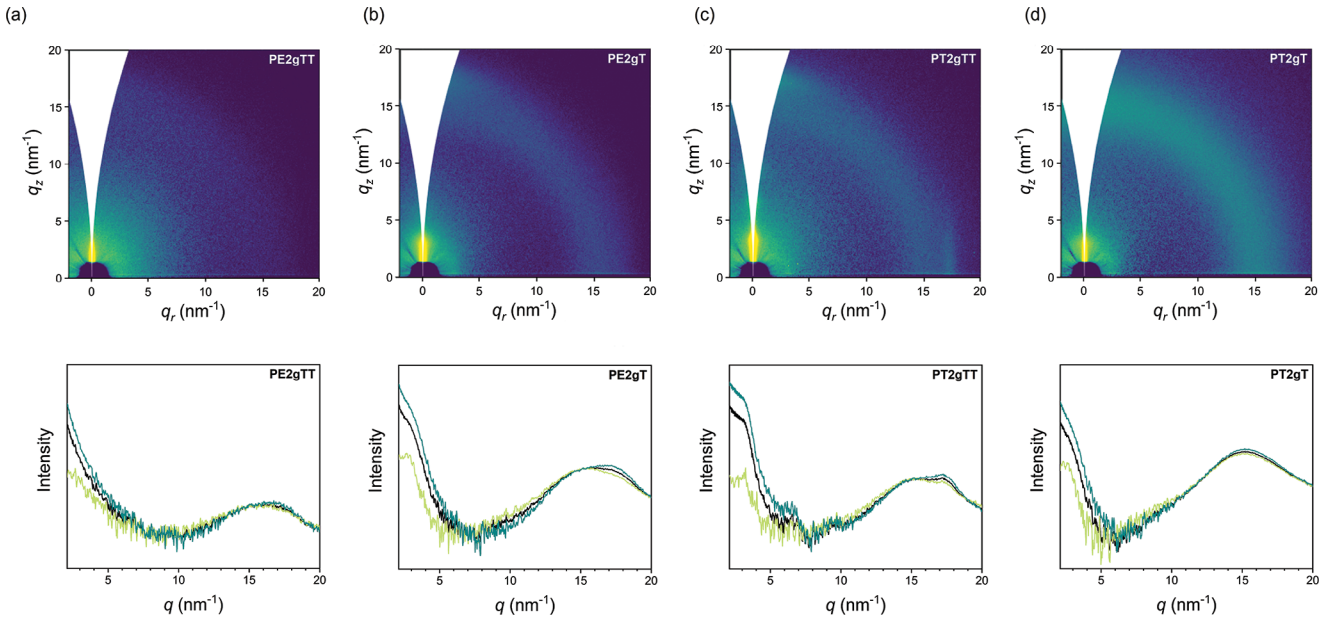

Figure 4. GIWAXS of a) **PE2gTT**, b) **PE2gT**, c) **PT2gTT,** and d) **PT2gT** dry films; with corresponding isotropic (black) and linecut integrations shown below, in the q_z (dark cyan, out of plane) and q_r (light green, in plane) directions.

peak along the q_z direction, at *d-spacing* = 0.36 nm. Thin films of **PT2gT** and OECT inoperable **PE2gTT** were found to be amorphous.

Electrolyte swelling of the active layer material in an OECT upon electrochemical biasing has a profound effect on device performance.[27,57,64] The swelling characteristics under electrochemical bias of **PE2gTT**, **PE2gT**, **PT2gTT**, and **PT2gT** films in 0.1 $_M$ KCl/H_2O were probed using an EQCM, for five CV cycles of applied potential between −0.8 and 0.8 V versus Ag/AgCl, at the scan rate of 100 mV/s (**Figure 5a**). Upon initial incrementation of the applied potential for **PE2gTT**, **PE2gT**, **PT2gTT**, and **PT2gT** films past their onset of oxidation up to 0.8 V, significant mass uptakes of varying degrees were observed for all four materials, assigned to the ingestion of anions and water by films for charge balancing electrochemical oxidation (hole injection). Upon further cycling from 0.8 back down to −0.8 V, a reversal in mass uptake was seen for all polymers, correlated to anion/water ejection commensurate with electrochemical de-doping (reduction). The baseline swelling of reduced films after the first cycle of applied potential were all higher (incrementing with each subsequent cycle) than that recorded for the pristine state at 0% mass uptake, owing to electrolyte retention within films.[65]

Peak mass uptakes at 0.8 V, representing absolute film swelling,[52] were seen to increase from **PT2gTT** < **PT2gT** < **PE2gTT** < **PE2gT** with average values of 40%, 55%, 56%, and 140% respectively. This observed trend in increasing EQCM peak mass uptakes reflects the proportionality of polar components in each materials design. Among the four polymers reported herein, **PE2gT** has the largest proportion of polar components drawing electrolyte into its films, with two triethylene

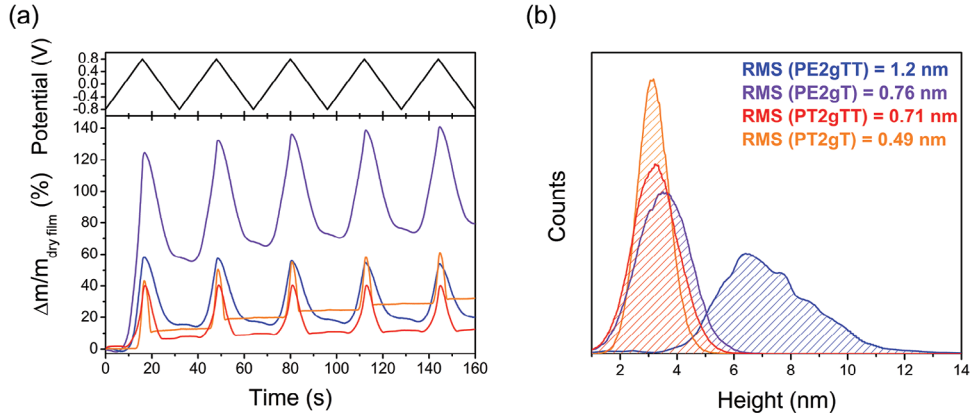

Figure 5. Thin film swelling and roughness data of **PE2gTT** (blue), **PE2gT** (violet), **PT2gTT** (red) and **PT2gT** (orange) showing a) fractional mass changes calculated from EQCM measurements in 0.1 $_M$ KCl/H_2O, with five cycles of potential applied shown at top (black), as well as b) RMS mean surface roughness from AFM images of pristine thin films.

glycol sidechains plus an ethylenedioxy bridge for each bisthiophene repeat unit, reasoning its highest peak EQCM mass uptake of 140%. The materials design of **PE2gTT** and **PT2gT** both feature a lower proportion of polar components compared to **PE2gT**, owing to the elongated thiophene-thienothiophene backbone repeat unit in **PE2gTT**, as well as the lack of an ethylenedioxy bridge in the repeat unit of **PT2gT** (c.f. **PE2gT**), explaining their lower peak EQCM mass uptakes. **PT2gTT** has the lowest proportion of two polar triethylene glycol sidechains within each thiophene-thienothiophene repeat unit, correlating with its peak EQCM mass uptake of 40% that is lowest among the four polymers tested. Differences in mass uptake between peak at 0.8 V and baseline swelling at −0.8 V (after the first cycle), representing active (bias-induced) film swelling only,[52] were calculated to be 40%, 75%, 30% and 30% for **PE2gTT**, **PE2gT**, **PT2gTT**, and **PT2gT** respectively.

Atomic-force microscopy images (AFM, Figure 5b; Figures S77–S80, Supporting Infromation) of **PE2gTT**, **PE2gT**, **PT2gTT**, and **PT2gT** thin films uncovered that OECT operable **PE2gT**, **PT2gTT**, and **PT2gT** all formed smooth thin films with RMS surface roughness values of 0.76, 0.71 and 0.49 nm respectively. On the other hand, **PE2gTT** formed rougher thin films with RMS surface roughness at 1.2 nm.

2.5. Discussion on Device Performance

Calculated OECT mobilities of **PE2gT**, **PT2gTT**, and **PT2gT** were found to correlate best with their degrees of polymerization. **PT2gT**, the polymer with the highest average molecular weight at M_n = 50 KDa, was calculated to exhibit the highest charge mobility in OECTs among all polymers tested. This is explained by the presence of effective electronic charge conduction pathways along long polymer strands within its thin films,[62,66] which act as tie-chains between crystalline domains and are less disrupted by thin film swelling upon electrochemical oxidation.[57] On the other hand, **PE2gT** with the largest EQCM peak electrolyte uptake at 140% upon electrochemical oxidation to 0.8 V versus Ag/AgCl and low average molecular weight of M_n = 3.6 KDa, was calculated to have the lowest OECT charge mobility, owing to disruption of confined charge conduction pathways by thin film electrolyte swelling.[66] **PT2gTT** with median average molecular weight of M_n = 11 KDa was determined to display an intermediary OECT charge mobility.

Volumetric capacitances of polymers studied were found to correlate best with the proportion of polar components in each materials design, which correlates with peak EQCM mass uptakes linked to electrolyte swelling. **PE2gT** with the biggest proportion of polar components per bisthiophene repeating unit, has a record volumetric capacitance of 313 F cm^{-3} (Table S1, Supporting Information), owing to its significant electrolyte swelling, which facilitate facile thin film counterion injection.[67–69] The removal of an ethylenedioxy bridge in the design of **PT2gT** (c.f. **PE2gT**) per bisthiophene repeating unit lowers the proportionality of polar components, correlating well with its comparatively decreased volumetric capacitance. **PT2gTT** has the lowest volumetric capacitance among the three OECT operational polymers reported herein, as it has the smallest glycol content per elongated thienothiophene-thiophene repeating unit.

Despite an electrochemically recorded onset of oxidation at −0.7 V versus Ag/AgCl, generation of sufficient, stable electronic charge carriers (holes) in **PE2gT** thin films to facilitate electronic conductivity, thereby turning its OECT(s) ON, is only achieved at a threshold voltage of −0.106 V, making **PE2gT** OECTs accumulation mode devices. This discrepancy between its oxidation onset and threshold voltage can be explained by the lack of chemically anchored counteranionic components in **PE2gT**, compromising the persistence of holes in its unbiased state and at cathodic (reductive) potentials. This counteranion phenomenon has been observed previously by Keene et al. for PEDOT:PSS, which feature the equivalent conjugated backbone as **PE2gT**, where treatment of PEDOT:PSS with various alkylamine based de-dopants that react with acidic PSS to form 1:1 cation-anion pair complexes results in a shift in OECT threshold voltages to accumulation mode operation, despite the de-doped PEDOT:PSS materials retaining onsets of oxidation at *ca.* −0.7 V versus Ag/AgCl.[18] The favourable accumulation mode OECT performance of **PE2gT** without the need for chemical de-doping, its straightforward two step synthesis with a good overall 34% yield,[46] as well as stable OECT performance with a μC* product figure-of-merit of 84.2 F cm^{-1} V^{-1} s^{-1} comparable to state-of-the-art PEDOT:PSS OECTs,[32,70] demonstrates potential for broader applicability of **PE2gT** in bioelectronics, as an alternative to PEDOT:PSS.

The minimal electrolyte swelling change of **PT2gT** films at potentials below (more cathodic than) ≈0.5 V versus Ag/AgCl (Figure 5a) is hypothesized to restrict counterion diffusion within its films, explaining the anomalous discrepancy between its solid state electrochemical onset of oxidation and DFT computed HOMO energy level.[52] The anodic onset of **PT2gT** film oxidation/lower OECT threshold voltage, alongside its high molecular weight, does endow good shelf life stability, owing to better resistance against ambient auto-oxidation and channel delamination.[16,61,62] In contrast, the higher cycling stability of **PE2gT** may be attributed to its higher OECT threshold voltage/more cathodic oxidation onset, which improves resilience of its oxidized state to redox side reactions with products of ORR.[63]

The inoperability of **PE2gTT** as an OECT material may be explained by its low molecular weight at M_n = 3.0 KDa and high surface roughness, which compromises thin film integrity upon swelling, causing delamination.

3. Conclusion

Motivated by a desire to create synthetically accessible p-type OMIECs for bioelectronics, we developed four glycolated polythiophenes, **PE2gTT**, **PE2gT**, **PT2gTT**, and **PT2gT**. All polymers were synthesized by atom-efficient direct arylation polymerization, circumventing the need for toxic organometallic precursors. Aqueous electrochemistry revealed **PE2gTT**, **PE2gT**, **PT2gTT**, and **PT2gT** onsets of oxidation at −0.5, −0.7, −0.2, and 0.3 V versus Ag/AgCl respectively. Overall, **PT2gT** displayed the champion accumulation mode OECT performance with an attained μC* product figure-of-merit of 290 F cm^{-1} V^{-1} s^{-1}, linked to its superior OECT charge mobility calculated at 1.00 cm^2 V^{-1} s^{-1} which is enabled by its high degree of polymerization (M_n = 50 KDa). A record volumetric capacitance among p-type glycolated polythiophene OMIECs of 313 F cm^{-3} was observed for **PE2gT**, which is explained by the high proportion of polar gly-

col and ethylenedioxy components in its materials design, that increases electrolyte swelling of its films upon electrochemical oxidation. The good OECT performance of **PE2gT** attaining a μC* product figure-of-merit of 84.2 F cm^{-1} V^{-1} s^{-1} that is comparable with state-of-the-art PEDOT:PSS devices, coupled with its favorable intrinsic accumulation mode operation and straightforward two-step synthesis with a sound overall yield of 34%, makes **PE2gT** a prime alternative to PEDOT:PSS in bioelectronics. Additionally, **PE2gT** OECTs with the least negative threshold voltage displayed the best operational cycling stability, owing to better resistance of its oxidized state against parasitic redox side reactions with products of the ORR, whilst **PT2gT** OECTs with the most negative threshold voltage and highest average molecular weight displayed better shelf life (unbiased) stability, attributable to better material resistance against ambient auto-oxidation and film delamination. Volumetric capacitances of **PE2gT**, **PT2gTT**, and **PT2gT** are all among the highest reported for glycolated polythiophenes, setting the precedent for their potential use in energy storage.

Supporting Information

Supporting Information is available from the Wiley Online Library or from the author.

Acknowledgements

The authors thank the Engineering and Physical Sciences Research Council (EPSRC) (EP/T028513/1) and KAUST baseline funding for support. B.D. acknowledges funding via the President's PhD Scholarship Scheme. V.L. and A.F.P. thank the National Science Foundation (NSF) through cooperative agreement number 1849213 for financial support. H. Y. acknowledges the PhD studentship support from the China Scholarship Council (CSC). J.N. and H.Y. thank the European Research Council for support under the European Union's Horizon 2020 research and innovation program (Grant Agreement No. 742708). J.N. thanks the Royal Society for award of a Research Professorship.

Conflict of Interest

There are no conflicts of interest to declare.

Data Availability Statement

The data that support the findings of this study are available from the corresponding author upon reasonable request.

Keywords

bioelectronics, organic electrochemical transistors, organic electronics, polymers, semiconductors

Received: October 31, 2023
Published online: January 23, 2024

[1] S. Inal, J. Rivnay, A.-O. Suiu, G. G. Malliaras, I. Mcculloch, *Acc. Chem. Res.* **2018**, *51*, 1368.
[2] E. Zeglio, A. L. Rutz, T. E. Winkler, G. G. Malliaras, A. Herland, *Adv. Mater.* **2019**, *31*, 1806712.
[3] B. D. Paulsen, K. Tybrandt, E. Stavrinidou, J. Rivnay, *Nat. Mater.* **2019**, *19*, 13.
[4] M. Moser, J. F. Ponder Jr, A. Wadsworth, A. Giovannitti, I. McCulloch, *Adv. Funct. Mater.* **2018**, *0*, 1807033.
[5] P. R. Paudel, J. Tropp, V. Kaphle, J. D. Azoulay, B. Lüssem, *J. Mater. Chem. C* **2021**, *9*, 9761.
[6] N. A. Kukhta, A. Marks, C. K. Luscombe, *Chem. Rev.* **2021**, *122*, 4325.
[7] P. Li, T. Lei, *J. Polym. Sci.* **2021**, *60*, 377.
[8] H. Jia, Z. Huang, P. Li, S. Zhang, Y. Wang, J.-Y. Wang, X. Gu, T. Lei, *J. Mater. Chem. C* **2021**, *9*, 4927.
[9] L. Bai, C. G. Elósegui, W. Li, P. Yu, J. Fei, L. Mao, *Front. Chem.* **2019**, *7*, 313.
[10] A. Nawaz, Q. Liu, W. L. Leong, K. E. Fairfull-Smith, P. Sonar, *Adv. Mater.* **2021**, *33*, 2101874.
[11] A. F. Paterson, H. Faber, A. Savva, G. Nikiforidis, M. Gedda, T. C. Hidalgo, X. Chen, I. Mcculloch, T. D. Anthopoulos, S. Inal, *Adv. Mater.* **2019**, *31*, 1902291.
[12] J. Rivnay, S. Inal, A. Salleo, R. M. Owens, M. Berggren, G. G. Malliaras, *Nat. Rev. Mater.* **2018**, *3*, 17086.
[13] D. A. Bernards, G. G. Malliaras, *Adv. Funct. Mater.* **2007**, *17*, 3538.
[14] E. Zeglio, O. Inganäs, *Adv. Mater.* **2018**, *30*, 1800941.
[15] J. Song, H. Liu, Z. Zhao, P. Lin, F. Yan, *Adv. Mater.* **2023**, 2300034.
[16] E. A. Schafer, R. Wu, D. Meli, J. Tropp, M. Moser, I. Mcculloch, B. D. Paulsen, J. Rivnay, *ACS Appl. Electron. Mater.* **2022**, *4*, 1391.
[17] A. F. Paterson, A. Savva, S. Wustoni, L. Tsetseris, B. D. Paulsen, H. Faber, A. H. Emwas, X. Chen, G. Nikiforidis, T. C. Hidalgo, M. Moser, I. P. Maria, J. Rivnay, I. Mcculloch, T. D. Anthopoulos, S. Inal, *Nat. Commun.* **2020**, *11*, 3004.
[18] S. T. Keene, T. P. A. Van Der Pol, D. Zakhidov, C. H. L. Weijtens, R. A. J. Janssen, A. Salleo, Y. Van De Burgt, *Adv. Mater.* **2020**, *32*, 2000270.
[19] M. Berggren, X. Crispin, S. Fabiano, M. P. Jonsson, D. T. Simon, E. Stavrinidou, K. Tybrandt, I. Zozoulenko, *Adv. Mater.* **2019**, *31*, 1805813.
[20] M. Elmahmoudy, S. Inal, A. Charrier, I. Uguz, G. G. Malliaras, S. Sanaur, *Macromol. Mater. Eng.* **2017**, *302*, 1600497.
[21] S.-M. Kim, C.-H. Kim, Y. Kim, N. Kim, W.-J. Lee, E.-H. Lee, D. Kim, S. Park, K. Lee, J. Rivnay, M.-H. Yoon, *Nat. Commun.* **2018**, *9*, 3858.
[22] Y. Kim, H. Noh, B. D. Paulsen, J. Kim, I.-Y. Jo, H. Ahn, J. Rivnay, M.-H. Yoon, *Adv. Mater.* **2021**, *33*, 2007550.
[23] X. Wu, M. Stephen, T. C. Hidalgo, T. Salim, J. Surgailis, A. Surendran, X. Su, T. Li, S. Inal, W. L. Leong, *Adv. Funct. Mater.* **2021**, 2108510.
[24] S. Tekoglu, D. Wielend, M. C. Scharber, N. S. Sariciftci, C. Yumusak, *Adv. Mater. Technol.* **2020**, *5*, 1900699.
[25] M. Ghazal, M. Daher Mansour, C. Scholaert, T. Dargent, Y. Coffinier, S. Pecqueur, F. Alibart, *Adv. Electron. Mater.* **2021**, 2100891.
[26] K. Janzakova, M. Ghazal, A. Kumar, Y. Coffinier, S. Pecqueur, F. Alibart, *Adv. Sci.* **2021**, *8*, 2102973.
[27] M. Moser, J. Gladisch, S. Ghosh, T. C. Hidalgo, J. F. Ponder, R. Sheelamanthula, Q. Thiburce, N. Gasparini, A. Wadsworth, A. Salleo, S. Inal, M. Berggren, I. Zozoulenko, E. Stavrinidou, I. Mcculloch, *Adv. Funct. Mater.* **2021**, *31*, 2100723.
[28] P. Schmode, A. Savva, R. Kahl, D. Ohayon, F. Meichsner, O. Dolynchuk, T. Thurn-Albrecht, S. Inal, M. Thelakkat, *ACS Appl. Mater. Interfaces* **2020**, *12*, 13029.
[29] A. Savva, R. Hallani, C. Cendra, J. Surgailis, T. C. Hidalgo, S. Wustoni, R. Sheelamanthula, X. Chen, M. Kirkus, A. Giovannitti, A. Salleo, I. Mcculloch, S. Inal, *Adv. Funct. Mater.* **2020**, *30*, 1907657.
[30] M. Moser, L. R. Savagian, A. Savva, M. Matta, J. F. Ponder, T. C. Hidalgo, D. Ohayon, R. Hallani, M. Reisjalali, A. Troisi, A. Wadsworth, J. R. Reynolds, S. Inal, I. Mcculloch, *Chem. Mater.* **2020**, *32*, 6618.
[31] L. R. Savagian, A. M. Österholm, J. F. Ponder, K. J. Barth, J. Rivnay, J. R. Reynolds, *Adv. Mater.* **2018**, *30*, 1804647.

[32] S. Inal, G. G. Malliaras, J. Rivnay, *Nat. Commun.* **2017**, *8*, 1767.
[33] J. C. Brendel, M. M. Schmidt, G. Hagen, R. Moos, M. Thelakkat, *Chem. Mater.* **2014**, *26*, 1992.
[34] E. Zeglio, M. Vagin, C. Musumeci, F. N. Ajjan, R. Gabrielsson, X. T. Trinh, N. T. Son, A. Maziz, N. Solin, O. Inganäs, *Chem. Mater.* **2015**, *27*, 6385.
[35] E. Zeglio, J. Eriksson, R. Gabrielsson, N. Solin, O. Inganäs, *Adv. Mater.* **2017**, *29*, 1605787.
[36] P. Schmode, D. Ohayon, P. M. Reichstein, A. Savva, S. Inal, M. Thelakkat, *Chem. Mater.* **2019**, *31*, 5286.
[37] A. T. Lill, D. X. Cao, M. Schrock, J. Vollbrecht, J. Huang, T. Nguyen-Dang, V. V. Brus, B. Yurash, D. Leifert, G. C. Bazan, T.-Q. Nguyen, *Adv. Mater.* **2020**, *32*, 1908120.
[38] Y. He, N. A. Kukhta, A. Marks, C. K. Luscombe, *J. Mater. Chem. C* **2022**, *7*, 2314.
[39] C. B. Nielsen, A. Giovannitti, D.-T. Sbircea, E. Bandiello, M. R. Niazi, D. A. Hanifi, M. Sessolo, A. Amassian, G. G. Malliaras, J. Rivnay, I. Mcculloch, *J. Am. Chem. Soc.* **2016**, *138*, 10252.
[40] A. Giovannitti, D.-T. Sbircea, S. Inal, C. B. Nielsen, E. Bandiello, D. A. Hanifi, M. Sessolo, G. G. Malliaras, I. Mcculloch, J. Rivnay, *Proc. Natl. Acad. Sci. U.S.A.* **2016**, *113*, 12017.
[41] M. Moser, T. C. Hidalgo, J. Surgailis, J. Gladisch, S. Ghosh, R. Sheelamanthula, Q. Thiburce, A. Giovannitti, A. Salleo, N. Gasparini, A. Wadsworth, I. Zozoulenko, M. Berggren, E. Stavrinidou, S. Inal, I. Mcculloch, *Adv. Mater.* **2020**, *32*, 2002748.
[42] M. Moser, Y. Wang, T. C. Hidalgo, H. Liao, Y. Yu, J. Chen, J. Duan, F. Moruzzi, S. Griggs, A. Marks, N. Gasparini, A. Wadsworth, S. Inal, I. Mcculloch, W. Yue, *Mater. Horiz* **2022**, *9*, 973.
[43] L. Lan, J. Chen, Y. Wang, P. Li, Y. Yu, G. Zhu, Z. Li, T. Lei, W. Yue, I. Mcculloch, *Chem. Mater.* **2022**, *34*, 1666.
[44] F. Lombeck, H. Komber, S. I. Gorelsky, M. Sommer, *ACS Macro Lett.* **2014**, *3*, 819.
[45] A. Luzio, D. Fazzi, F. Nübling, R. Matsidik, A. Straub, H. Komber, E. Giussani, S. E. Watkins, M. Barbatti, W. Thiel, E. Gann, L. Thomsen, C. R. Mcneill, M. Caironi, M. Sommer, *Chem. Mater.* **2014**, *26*, 6233.
[46] B. Ding, G. Kim, Y. Kim, F. D. Eisner, E. Gutiérrez-Fernández, J. Martín, M.-H. Yoon, M. Heeney, *Angew. Chem., Int. Ed.* **2021**, *60*, 19679.
[47] R. Matsidik, H. Komber, A. Luzio, M. Caironi, M. Sommer, *J. Am. Chem. Soc.* **2015**, *137*, 6705.
[48] R. Matsidik, J. Martin, S. Schmidt, J. Obermayer, F. Lombeck, F. Nübling, H. Komber, D. Fazzi, M. Sommer, *J. Org. Chem.* **2015**, *80*, 980.
[49] M. Wakioka, Y. Nakamura, M. Montgomery, F. Ozawa, *Organometallics* **2015**, *34*, 198.
[50] K. Nakabayashi, *Polym. J.* **2018**, *50*, 475.
[51] G. Conboy, H. J. Spencer, E. Angioni, A. L. Kanibolotsky, N. J. Findlay, S. J. Coles, C. Wilson, M. B. Pitak, C. Risko, V. Coropceanu, J.-L. Brédas, P. J. Skabara, *Mater. Horiz* **2016**, *3*, 333.
[52] A. A. Szumska, I. P. Maria, L. Q. Flagg, A. Savva, J. Surgailis, B. D. Paulsen, D. Moia, X. Chen, S. Griggs, J. T. Mefford, R. B. Rashid, A. Marks, S. Inal, D. S. Ginger, A. Giovannitti, J. Nelson, *J. Am. Chem. Soc.* **2021**, *143*, 14795.
[53] B. Ding, B. Chan, N. Proschogo, M. B. Solomon, C. J. Kepert, D. M. D'alessandro, *Chem. Sci.* **2021**, *12*, 3608.
[54] D. Moia, A. Giovannitti, A. A. Szumska, I. P. Maria, E. Rezasoltani, M. Sachs, M. Schnurr, P. R. F. Barnes, I. Mcculloch, J. Nelson, *Energy Environ. Sci.* **2019**, *12*, 1349.
[55] C. Cendra, A. Giovannitti, A. Savva, V. Venkatraman, I. Mcculloch, A. Salleo, S. Inal, J. Rivnay, *Adv. Funct. Mater.* **2019**, *29*, 1807034.
[56] B. T. Ditullio, L. R. Savagian, O. Bardagot, M. De Keersmaecker, A. M. Österholm, N. Banerji, J. R. Reynolds, *J. Am. Chem. Soc.* **2023**, *145*, 122.
[57] L. Q. Flagg, C. G. Bischak, J. W. Onorato, R. B. Rashid, C. K. Luscombe, D. S. Ginger, *J. Am. Chem. Soc.* **2019**, *141*, 4345.
[58] M. Zhu, P. Li, J.-L. Li, T. Lei, *Mol. Syst. Des. Eng.* **2022**, *7*, 6.
[59] L. Q. Flagg, R. Giridharagopal, J. Guo, D. S. Ginger, *Chem. Mater.* **2018**, *30*, 5380.
[60] M. M. Schmidt, M. Elmahmoudy, G. G. Malliaras, S. Inal, M. Thelakkat, *Macromol. Chem. Phys.* **2018**, *219*, 1700374.
[61] A. Giovannitti, R. B. Rashid, Q. Thiburce, B. D. Paulsen, C. Cendra, K. Thorley, D. Moia, J. T. Mefford, D. Hanifi, D. Weiyuan, M. Moser, A. Salleo, J. Nelson, I. Mcculloch, J. Rivnay, *Adv. Mater.* **2020**, *32*, 1908047.
[62] H.-Y. Wu, C.-Y. Yang, Q. Li, N. B. Kolhe, X. Strakosas, M.-A. Stoeckel, Z. Wu, W. Jin, M. Savvakis, R. Kroon, D. Tu, H. Y. Woo, M. Berggren, S. A. Jenekhe, S. Fabiano, *Adv. Mater.* **2021**, *34*, 2106235.
[63] S. Zhang, P. Ding, T.-P. Ruoko, R. Wu, M.-A. Stoeckel, M. Massetti, T. Liu, M. Vagin, D. Meli, R. Kroon, J. Rivnay, S. Fabiano, *Adv. Funct. Mater.* **2023**, 2302249.
[64] A. Savva, C. Cendra, A. Giugni, B. Torre, J. Surgailis, D. Ohayon, A. Giovannitti, I. McCulloch, E. Di Fabrizio, A. Salleo, J. Rivnay, S. Inal, *Chem. Mater.* **2019**, *31*, 927.
[65] L. Q. Flagg, C. G. Bischak, R. J. Quezada, J. W. Onorato, C. K. Luscombe, D. S. Ginger, *ACS. Mater. Lett.* **2020**, *2*, 254.
[66] J. Tropp, D. Meli, R. Wu, B. Xu, S. B. Hunt, J. D. Azoulay, B. D. Paulsen, J. Rivnay, *ACS Mater. Lett.* **2023**, *5*, 1367.
[67] G. Lecroy, C. Cendra, T. J. Quill, M. Moser, R. Hallani, J. F. Ponder, K. Stone, S. D. Kang, A. Y.-L. Liang, Q. Thiburce, I. Mcculloch, F. C. Spano, A. Giovannitti, A. Salleo, *Mater. Horiz.* **2023**, *10*, 2568.
[68] D. Ohayon, V. Druet, S. Inal, *Chem. Soc. Rev.* **2023**, *52*, 1001.
[69] T. J. Quill, G. Lecroy, D. M. Halat, R. Sheelamanthula, A. Marks, L. S. Grundy, I. Mcculloch, J. A. Reimer, N. P. Balsara, A. Giovannitti, A. Salleo, C. J. Takacs, *Nat. Mater.* **2023**, *22*, 362.
[70] J. Tropp, D. Meli, J. Rivnay, *Matter* **2023**, *6*, 3132.